Original Research Article

J. Funct. Mater. Biomol. 7(2) (2023) pp 721 – 729

Journal of Functional Materials and Biomolecules

Journal homepage: www.shcpub.edu.in

ISSN: 2456-9429

STRUCTURAL AND ANTIBACTERIAL STUDY OF TITANIUM DIOXIDE NANOPARTICLES WITH THE IMPACT OF AMINO-ACIDS BY CONVECTION MICROWAVE IRRADIATION METHOD

Ameer Baig Ali Baia[1]*, Velukumar Ramya[1]

Received on 21 November 2023, accepted on 30 November 2023,
Published online on December 2023

Abstract

In this present analysis, the Titanium dioxide (TiO_2) nanoparticles (NPs) and theiramino - acids (glycine and alanine) influenced TGA NPs were effectually synthesized by microwave irradiation method also with high temperature. The impression of amino - acids supported as - synthesized TGA NPs has characterized by XRD, FTIR, UV-VIS, FE-SEM analysis for structural, optical analysis, and specific antibacterial activities. Since the crystal structure consumingthe (hkl) orientation with the crystallite size (D), dislocation density (δ), strain, specific surface area (SSA) their inter relationships of morphology index (M.I.) were calculated. The defined functional groups were attained by various modes of vibration are exposed through FT-IR spectra analysis. The optical absorption fascination ability and bandgap (Eg) of the as-obtained TiO_2 and TGANPs were intended by UV-Visible spectra analysis. As-obtained TiO_2 and TGANPs were originated to be the spherical shape and agglomerated surface morphology from the FESEM analysis. Likewise, the enhanced antibacterial activity based on the zone of inhibition (ZOI) for gram-negative (G-) E. Coli microbesillustrates with high calcination (600°C) temperature of amino-acid coupled TGA NPs was deliberated.

Keywords: Antibacterial activity; Titanium dioxide; Nanoparticles; Amino-Acids; Microwave Irradiation; Glycine and Alanine; High Temperature.

1. Introduction

Nanotechnology is anemergentfield as a quickly growing areaof its application for manufacturing novelnanomaterials (NMs) at the nanoscaleseries [1]. Emerging antibiotic resistance to bacterial is a foremost medical task. The explorationof drugs bynovelbehaviours of their exploited and thusexcessiveconcern for the pharmacological and research societies [2]. Medicinal plants and antibiotic nanomaterials are two promisingcauses of the unique antimicrobial mediators. The antibacterial properties of NMsand also the activemetal nanoparticles (NPs) could be owing to numerousappliances such as the invention of reactive oxygen species (ROSs), inactivation of cellular enzymes, and nucleic acids of the microberesultant forthe pore realization into the bacterial cell-wall. Titanium dioxide (TiO_2) NPs iscategorizedamong the several metal NPs, because of cost-effective, high stability, harmless, and environment friendly etc.,[3, 4]. Also, TiO_2 has aneffective photocatalyst and extensively used for self-cleaning and/or self-disinfecting substantive for surface coating in various applications. Similarly, theTiO_2 NPs showed a furtherbeneficial role in ecologicalrefinement and its super-hydrophobicity, anti-fogging propertiesof photo-excited and eco-toxicological evaluation, expresslythe nano-sized TiO_2 have executed on severalmodels, such as plants, microbes, and the animal natures [5]. Likewise, TiO_2 is an inorganic white solid compact ingredient, chemically inert complex, which ensues in the mineral soils and also severaltypes of rocks reasonably.

In a scientifically enabled society, the TiO_2 NPs had engaged a prominent place. As the titanium (IV) isopropoxide would respond by water, and to get the TiO_2. Usually, the reaction process was involved in synthesizing TiO_2 NPs are significant applications in numerous fields alsoon sustainable [6, 7], which could efforts to diminish the destructive substances with amino acids based modifications [8]. While, the TiO_2 has to be three phases such as rutile, anatase, and brookite [5-7]. For anatase TiO_2 NMs have extensive industrial uses, apply for obvious biological activity, which further toxic than the rutile and brookite system of TiO_2 [9]. In the exploit, this approach has feasibly for the binding of various energetic amino acids linked metal-ions, which expected to potential applications with biological activity. This amino-acid has a crucial substrate for the production of numerous biologically imperative biomolecules and compounds [10]. Though the glycine is minutest, significant, neutral, and metabolically inactive amino-acid, also a carbon atom assured to two hydrogen atoms, to an amino pairwith carboxyl group equally [11]. Further, it has a wide variety of cytoprotective, immune-modulatory, and anti-inflammatory properties [12].

***Corresponding Author email:** ameerramphysics@gmail.com
[1]Department of Physics, St. Joseph College of Arts and Science For Women, Pagalpatty-666304, Omalur (tk), Salem, TamilNadu, India.

Meanwhile, alanine is an α-amino acid has used in the biosynthesis of protein research. Also, it comprises an amine, carboxylic acid and the crucial carbon atom which also transfers a methyl group side chain linked relatively [13]. Hence, the effortto create for the amino-acids achieved TiO_2 NPs has penetrated the enhanced antibacterial activity with superior structure stability [14,15].

Hence, the present work has been considered that the properties of aminoacids (glycine and alanine) performed TiO_2 NPs on its antibacterial activity. Since the amino acids have interacted with the specified TiO_2 NMs, also study its structural, morphologies and optical absorption properties [11]. Thus, the definition of glycine and alanine have moral sources of N, C and H sources have a perfect mediator which might cause a stable compound by the carbon nano-cage over its amino nitrogen dynamic site. Further, the glycine and alanine functionalization of TiO_2 NPs could expand its photochemical and ability for bactericidal performance.

2. Experimental procedures

2.1. Materials

Titanium (IV) isopropoxide (TTIP), amino-acids (like glycine and alanine), ethanol absolute, ammonia (NH_3) solution, de-ionized (D.I.) water and acetone etc.

2.2. Preparation process of TiO_2nanomaterial

All the chemical substances used forthe experimental process of analytical reagent grade (A.R) and were used without auxiliary refinement. Initially, the 0.5 M of TTIP was dissolved in100 mL of D.I. water, thus taken in vigorous stirring for 45 minutes [8]. Since theTTIP has reacted with H_2O to form the TiO_2 nanomaterial through the soft white precipitates, then 2 drops of NH_3 solution were added to sustain the pH range at ~8. Later, the colloidal white precipitate was reserved in an undisturbed form. The attained TiO_2 precipitate was again washed for further purification, with ethanol (5 mL) and D.I. water (45 mL) mixed solution (1:9), concurrently. Additionally, the microwave irradiation was passed through the TiO_2 white precipitate and then heat at 110° C for 1 hour by the microwave conventional approach [9]. Lastly, obtained pure TiO_2 nanopowders (NPs) were further annealed in a muffled furnace at 600° C for 3hours.

2.3.Preparation of amino-acids influenced TiO_2 (TGA) nanomaterials

For the preparation of amino-acids (glycine and alanine) influenced TiO_2 NP having the same reaction process of pure TiO_2 NPs were surveyed. Then the 0.02 M of both glycine and alanine were taken into dissolution in 50 mL of D.I. water, and then it has further drop-wise mixed to the afore said precursor solution for functionalizing the TiO_2 solution [11], and then keep into the microwave irradiation progress. Finally, the as-obtained amino-acids influenced TiO_2 (TGA) nanomaterial were further annealed in a furnace at 600° C for 3 hours. The as-obtained high-temperature TGA nanomaterial was further characterized by UV-Vis, FT-IR, FESEM, XRD and also the antibacterial activities.

2.4 Characterization techniques

The crystalline structure, phase purity and crystallite size of as-obtained TiO_2 and TGA nanomaterials have analyzed using powder X-Ray (XRD) diffractometer by Brukar tensor extent over monochromatic CuKα radiation and in a range of 10-80°. To evaluate the chemical interfaces of functional groups were evaluated by Fourier transform infrared (FT-IR) spectra studiesusing Perkin Elmer RX-1 brand spectrophotometer The field emission scanning electron (FESEM) microscope is a valuable system to define the surface morphologies of the as-given nanomaterial. The optical absorption properties and their related direct and indirect bandgap (E_g) energy values were organized via UV-Vis diffuse reflectance spectrophotometer (UV-Vis DRS; Perkin Elmer UV/Vis Lambda 19) at the wavelength of 200-800 nm.

2.5 Antibacterial activity

To understand the antibacterial performance ofas-synthesized TiO_2 and TGA NPs were measured by typical agar well diffusion method [16, 17], using gram-negative (G^-) *Escherichia coli* (*E. coli*) bacteria as a test bacterium. The bacterium was grown in Brain Heart Infusion (BHI) broth and diluted to around 10^5 colony-forming units (CFU)/mL, and the culture was flooded-inoculated onto the surface of Mueller Hinton agar moderate. The 5 mm diameter wells were cut since the agar by a sterile cork-borer and 30 µL (5 µg compound is widespread in 500 µL of DMSO) of the sample solution were poured into the wells, further the plates were incubated for 24 h at 37 °C constantly [18]. Antibacterial activity was evaluated by the diameter of zone of inhibition (ZOI) in mm range against the *E. coli* bacteria and the DMSO were used as solvent control.

3.Results and Discussion

3.1 Ultra violet-visible (UV-Vis) absorption spectra analysis

The optical properties and the bandgap(E_g) energyof the as-prepared TiO_2 and T:G:A nanomaterials were determined using UV-Vis absorption spectra [19] and hence they verified in the ~200-800 nm wavelength range. Since Figure. 1, the cutoff wavelength would start sharply inthe ~220 nm for TiO_2 and increases to ~230 nm for TGA NPs exclusively. Because of this, the amino-acids were incorporated in the TiO_2 surfaces, which might improve the optical absorption properties respectively. Also, the absorption coefficient (α) has associated with the bandgap (E_g) was calculated by the subsequent expression in Eqn. 1, 2 and 3;

$$(\alpha h\nu)^2 = B\,(h\nu - E_g)^n \quad (1)$$

$$E_g = hc/\lambda \quad (2)$$

$$I = I_0\, e^{-\alpha t} \quad (3)$$

Where, h, α, ν, c, λ, B, I, I_o and t stands for plank's constant (6.626 x 10^{-34} Js.), optical absorption coefficient, photon

frequency, speed of light (3 x 10^8 ms^{-1}), cut-off wavelength (410.57 x 10^{-9} m), relatively constant, the intensity of transmitting light, the intensity of incident light and the further thickness of the specified samples respectively.

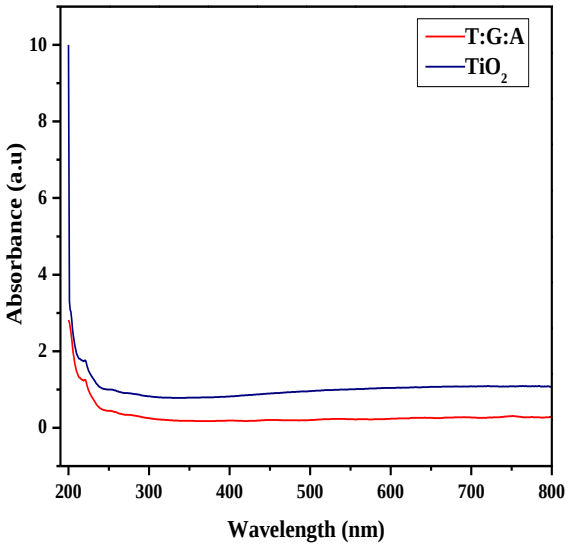

Figure. 1. UV-Vis absorption spectra of as-synthesized TiO_2 and TGAnanomaterials

Figure. 2 (A) and (B) signified for the Tauc plots of direct and indirect energy gap (Eg) for the as-synthesized TiO_2

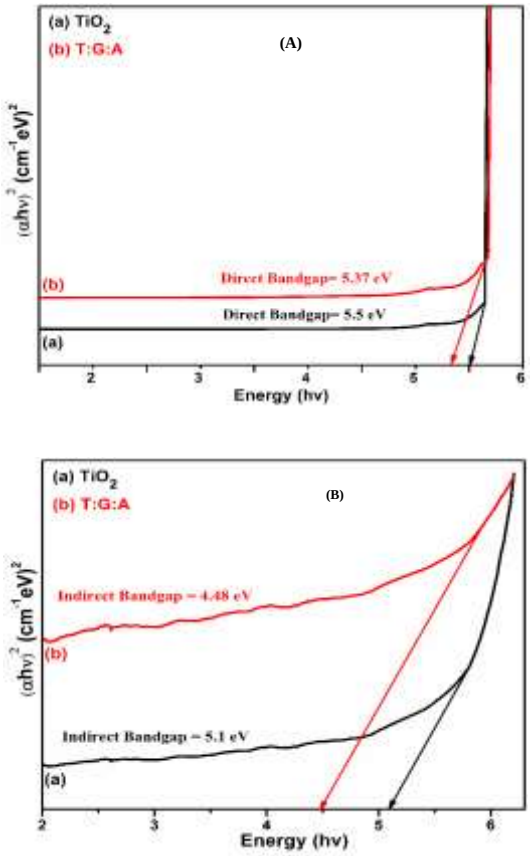

Figure.2. Tauc plots of (A) direct and (B) indirect bandgap for the as-synthesized NPs

and TGA nanomaterials, relatively. From the Tauc-plot (Figure.2(A)) of indirect bandgap energy (Eg) for TiO_2 nanoparticle (5.5 eV) was shifted to ~5.37eV after influencing with amino-acids united TGA nanomaterial. Likewise, the direct energy gap (Eg) for TiO2 NPs was shifted from ~5.1 to 4.48 eV for TGA NPs as exposed in Figure. 2 (B). Optical bandgap (Eg) has declined by increasing particle size owing to quantum size possessions [9, 19]. The number of overlying through theorbits or energy-level was declining and the width of bandgap would obtainthe narrower, henceowed to the influence of amino-acids over the bandgap of TiO_2 NPs. This indicates a red shift (bathochromic shift) of the optical absorption spectrum towards the upper wavelength expanse.

3.2. FT-IR spectra analysis

The obtained functional vibration groups were specifying that the specified TiO2 and TGA compounds have been analyzed by FT-IR spectra are revealed in Figure. 3. The strong peaks around 605 cm-1 in the FT-IR spectra authorize the O-Ti-O bond for the TiO2 based nanomaterials [20]. Since Figure. 3 (a), it has perceived that the FT-IR spectrum of as-obtained TGA NPs has several further vibrations that were a manifestation of amino acids like glycine and alanine is an association in the TiO2 NPs(Figure. 3(b)). The occurrence of glycine in a broad intensity at 2866 cm-1 by for carboxylic-acids (RCO2H) structure, and also the range at 3383 cm-1 consigned in O-H bend, H-bond and N-H stretch for C=CCOOH structure of the as-attained nanomaterials [20]. In the incidence of alanine, the complex was acquired into medium strengths at 3292 cm-1 allotted in for =C-H and -C≡C-H stretches for alkynes depots, similarly in the series of 1635 cm-1 for N-H bending vibrations of -CO-NH- structure. The occurrence of TiO2 nanomaterial has established by the robust peaks at the range of 534 cm-1 for alkyl halides (C-Br stretch), at 3433 cm-1 for -OH stretches [21] and the 2920 cm-1 series of -OH by detailed carboxylic acids (RCH_2CH_3) functions individually. Thus, the authorize on frequent functional groups of arranged compounds would presents in the as-synthesized TiO2 and TGA nanomaterials respectively.

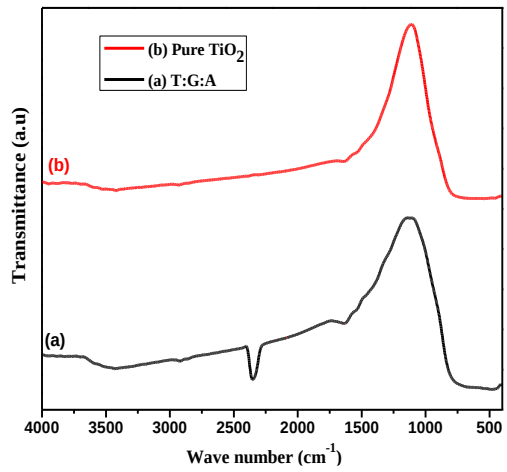

Figure. 3 FT-IR spectra for as-synthesized (a) TGA and (b) TiO_2NPs

3.2. Field Emission Scanning Electron Microscope (FESEM) analysis

The surface morphology and microstructures of as-synthesized TiO_2 and TGA NPs were attained via FESEM

analysis and typical pictures are obtainable in high/different magnification as in Figure. 4 (a-d). The specified both TiO_2 and TGA NPs were agglomerated nature by uniformly distributed substances were observed and originate to be circular shape also found in the micrographs. Compared with TiO_2 images, the TGA nanomaterial was highly agglomerated with even spherical shaped nanostructure respectively [22, 23]. Moreover, the consistent distribution by agglomerated NPs has enabled decent bacterium-particle contact which is beneficial for antibacterial activity.

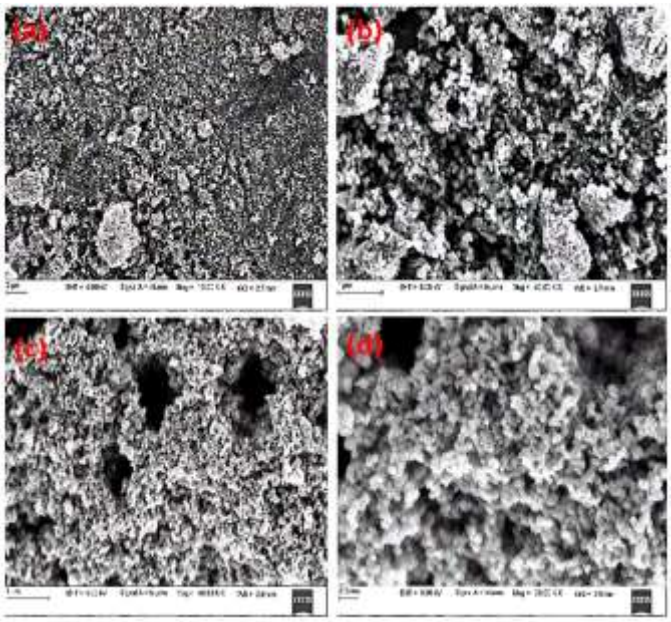

Figure. 4 FESEM micrographs of as-obtained (a, b) $TiO_2$and (c, d) TGA nanomaterials

3.3. Structural investigation of TiO_2 and TGANPs by XRD analysis

The crystalline structure and phase purity ofas-obtained TiO_2 and TGANPs were established from the powder XRDpattern as publicized in Figure 5.The XRD pattern of Figure. 5 displays a tetragonal structured and anatase phase of TiO_2 and TGA NPs together; hence it has well-matched with the orientation of the hkl values with the standard JCPDS card file (01-0562) [8], and the planes (101), (103), (200), (105), (213), (116), (107) are gained at the position of 2θ = 25.281°, 37.934°, 48.376°, 53.884°, 62.999°, 68.998° and 75.374° respectively. Also, the lattice parameters of as-obtained TiO_2 NPs was a = b= 3.7750 Å, c 9.4900 = Å and the TGANPs has an a = b= 3.7300 Å, c = 9.3700 Å (a = b ≠ c)exclusively. The lattice angles for both TiO_2 and TGANPswere decidedby α = β = γ= 90˚, which specifies that the togetheras-obtained NPs has a tetragonal crystalline structure [24, 25]. The (101) plane hasdenotedthat the solid peak is determined at 24.98° position by calculating the FWHM (β) for fine crystalline NPs.

Crystallite Size (D) calculation: Since this reading, the intensity ofpowder XRD peaks is situated at 2θ, and the average crystalline size of as-obtainedNPswas appraised by the Debye-Scherer formula using a major (101) planes of both TiO_2 and TGA nanomaterials. Also, the inter-planar spacing amidthe d-spacing was intendedby Bragg's law and hence the termsof equations (4) and (5)as formerlyrecognized[27].

$$2d \sin\theta = n\lambda \quad \text{------- (4)}$$

$$D = 0.9\lambda / \beta \cos\theta \quad \text{-------- (5)}$$

Where D, λ, β and θ have stood for the crystallite diameter, a wavelength of X-Ray (0.1540 nm), FWHM (Full-width half maximum of itemized peak), diffracted angle. The intensity of the TiO_2 increases related to the TGA NPs with detail to the 2θ.Using the Scherrer formula, it has to originate that the typical crystallite size condensed from 37.65 nm for TiO_2 owing to the impact of amino-acids to 33.89 nm for TGA NPs. The perceived lesser crystalline size of TGA NPs might be owing to the impact of amino-acids were touching in the interstitial places and/or substitutions situates of the TiO_2 crystalline lattice [28]. The minor crystalline size besides the perceived greatly energetic anatase phase of TiO_2 NPs benefits the microbial cell wall penetrating also proficiently killing the bacteria.

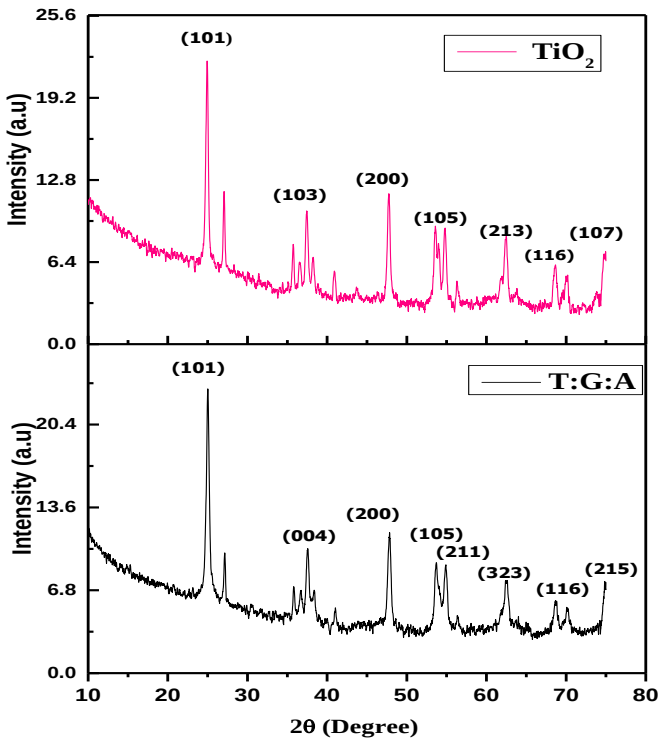

Figure. 5 XRD pattern of as-synthesized TiO_2 and TGA NPs

Williamson-Hall Plot

Williamson-Hall design was used to estimate for crystallite size and lattice strain of the as-obtained NPs using the succeeding expression (6). The entire widening XRD diffraction peak are owing to the as-obtained NPs by β_t equation as previously defined [29] and specified as follows in equation (6),

$$B_t = B_{Strain} + B_{Size} = \left\{\frac{K\lambda}{L\cos\theta}\right\} + \{4C\varepsilon \tan\theta\} \quad \text{------ (6)}$$

$$B_t \cos\theta = 4C\varepsilon \sin\theta + \frac{K\lambda}{L\cos\theta} \quad \text{------ (7)}$$

Where Cε, L, B_{Strain}, λ, K and θ were standing for the lattice strain, average crystallite size, strain widening, crystallite size widening, X-ray wavelength (1.5406 Å), dimensionless feature (0.9) and the Bragg angle in degrees. Also, the W-H plot is revealed in Figure. 6, hence it has designed by the graph of (B_t) cosθ besides the 4sinθ. The equation (7) has grown by the cosθ to crop, whereas the crystalline size could be projected from intercept $(\frac{K\lambda}{L})$. Though the lattice strain value was amplified from 0.133 (TiO_2) to 0.60215 (TGA) NPs in the major planes of (101) orientations for both samples, thus it might be owed to the quantum confinement influence. Still, the strain assessment upsurges for declining the crystallite size of as-obtained TiO_2 and TGA NPs together.

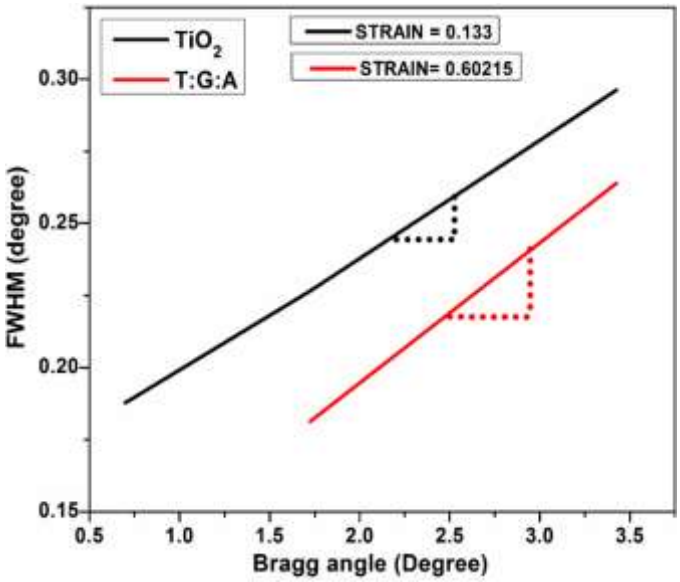

Figure. 6. Williamson Hall plot for as-synthesized (a) TiO_2 and (b) TGA NPs

Specific surface area (SSA) calculation

The specific surface area (SSA) plays asignificantpart in the specified NPsowed to their superior surface to volume ratio with a decrease in thecrystallite size, also, the SSA is used to define the absorption, heterogeneous catalysts and responses on surface possessions of distinct NPs [30]. The regularspecific surface area of as-obtained TiO2 and TGANPswas calculated by equation (8) which arethe values are accessible in Tables 1 and 2.

$$SSA = \frac{6000}{D*\rho} \quad \text{------- (8)}$$

WhereverD and ρ are the crystallite size and density of the as-obtained samples moderately. The typical specific surface area has initiated to be 2.40136 m2g-1for TiO2 and 2.11266 m2g-1 for TGA NPs, although the plot is clarified in the Figure.7. Also, they have exposed that the crystalline boundary size has amplifiedbyamassedthat the specific surface area, outstanding to the impact of amino-acids, while the hardness and solidity of TiO2NPs were enlarged [31].

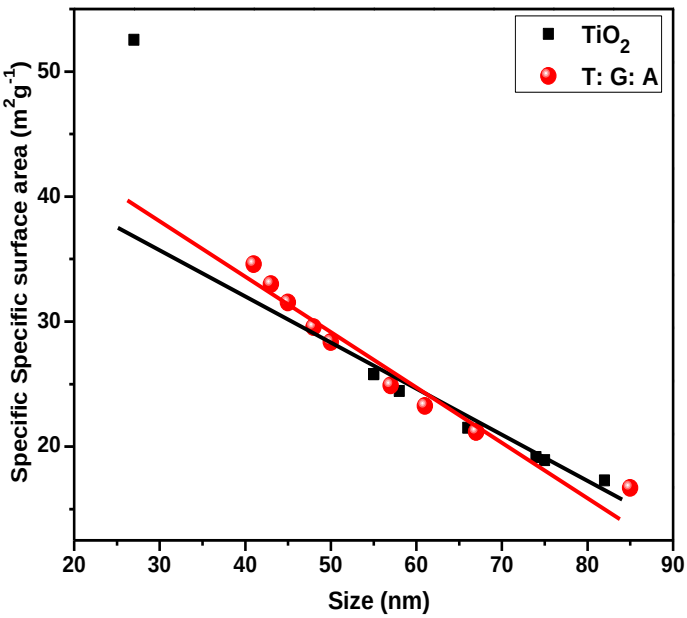

Figure.7 Specific surface areavs. size of as-synthesizedTiO_2 and TGA NPs

Dislocation Density (δ) Calculation

The dislocation density (δ) is the length of dislocation lines per unit volume of the as-obtained TiO_2 and TGA NPs. Larger dislocation density involves a greater hardness [20]and the calculateddataweretabularized in Tables 1 and 2.

$$\delta = \frac{15\beta\cos\theta}{4\alpha D} \quad \text{------- (9)}$$

$$\delta = 1 / D^2 \quad \text{------- (10)}$$

Wherever, δ, D, θ and β dislocation density, crystallite size, diffraction angle, the lattice constant in nm series and diffraction widening (radian) also. The dislocation density (δ) in the as-obtained TiO_2 and TGA NPs by the expressions (Eqn. 9 and 10) were determined as 7.304 x $10^{15}m^{-2}$forTiO_2 and 9.182 x $10^{15}m^{-2}$ for TGANPsas publicized in the Figure. 8. Dislocation density and strain were enlarged when crystallite size is also declining, the hardness and the strength are improvedin TGA than that of TiO_2NPs sensibly.

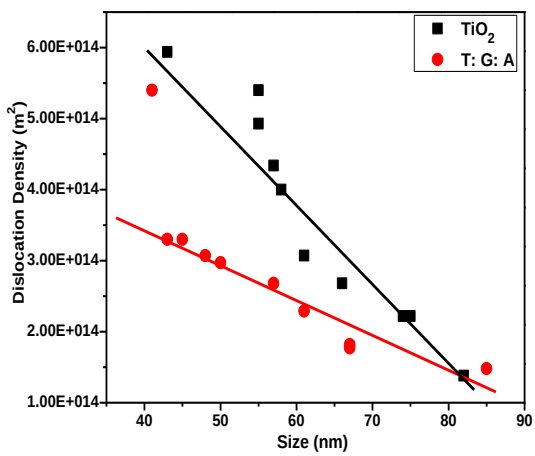

Figure.8 Dislocation density vs. size of as-synthesized TiO_2 and TGA NPs

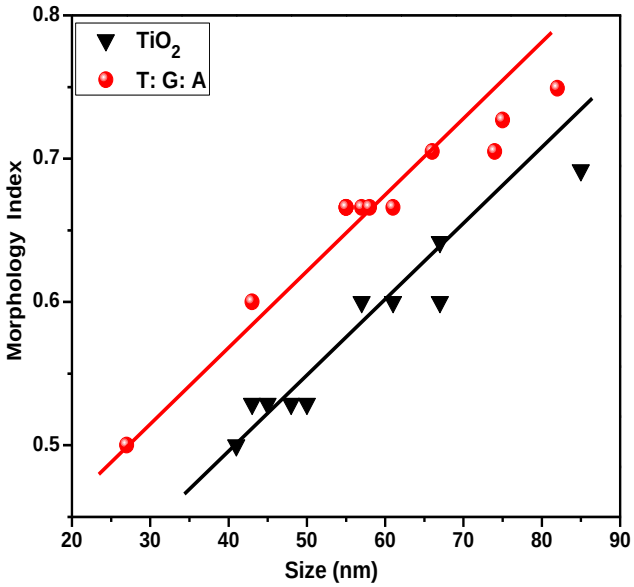

Figure.9 M.I vs. Size of as-obtained TiO_2 and TGA NPs

Table. 1 SSA, MI and dislocation density of the as-obtained TiO_2 NPs

Position [°2θ]	FWHM β [rad]	Size nm	SSA (m^2g^{-1})	MI (No Unit)	δ (m^2)
24.98	0.0020	67	21.17	0.642	2.22E+14
27.09	0.0016	85	16.68	0.692	1.38E+14
35.78	0.0025	57	24.88	0.6	3.07E+14
36.66	0.0033	43	32.98	0.529	5.40E+14
37.50	0.0033	43	32.98	0.529	5.40E+14
47.76	0.0033	45	31.52	0.529	4.93E+14
53.61	0.0025	61	23.25	0.6	2.68E+14
54.83	0.003	41	34.59	0.5	5.94E+14
62.41	0.0033	48	29.55	0.529	4.34E+14
68.56	0.0033	50	28.36	0.529	4.00E+14
70.07	0.0025	67	21.17	0.6	2.22E+14

Table. 2 SSA, MI and dislocation density of the as-obtained TGA NPs

Position [°2θ]	FWHM β [rad]	Size nm	SSA (m^2g^{-1})	MI (No Unit)	δ (m^2)
24.920	0.0018	75	18.91	0.727	1.77E+14
27.032	0.0020	66	21.49	0.705	2.29E+14
35.700	0.0025	57	24.88	0.666	3.07E+14
36.539	0.0025	55	25.78	0.666	3.30E+14
37.379	0.0033	43	32.98	0.6	5.40E+14
38.160	0.0025	55	25.78	0.666	3.30E+14
40.859	00025	58	24.45	0.666	2.97E+14
47.691	0.0251	55	25.78	0.666	3.30E+14
53.518	0.0251	61	23.25	0.666	2.68E+14
53.960	0.0067	82	17.29	0.749	1.48E+14
54.715	0.0029	74	19.16	0.705	1.82E+14
56.341	0.0050	27	52.53	0.5	1.37E+14

Morphology index (M.I) calculation

The as-obtained $TiO_2$and TGANPs wereextensively used in various diverse industries, and similarly, such applications have resulted fromtheirexclusive structural, chemical and physicalbelongings, which are replicated by theirstability, surface things, crystalline size and morphology too. It has planned that the SSA of TiO_2 NPs is governed by the interrelationships of particle, morphology and size [32]. A morphological directory is gained using the equation (11) andobtained complete ideals are computed in Table. 1 and 2.

$$M.I = \frac{FWHM_h}{(FWHM_h + FWHM_p)} \quad \text{------- (11)}$$

Where M.I, $FWHM_h$ and$FWHM_p$ are stances for morphology index, highest FWHM value and the particular peak's FWHM, which are into M.I arealso to be intended.

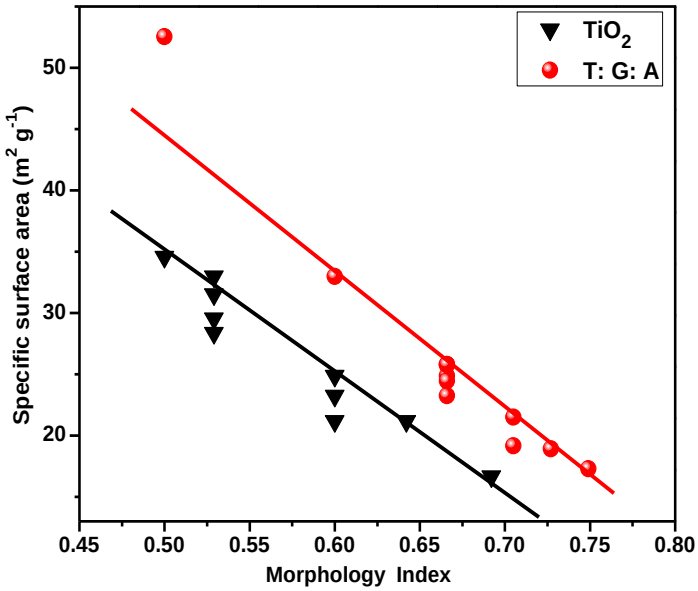

Figure. 10 MI vs. SSA of the as-obtained TiO_2 and TGA NPs

Figure. 9, denotes the chartamong the M.I and crystallite size of the as-obtained TiO_2 and TGA NPs separately. The M.I range of as-obtained TiO_2NPs has from 0.5-0.6542 and 0.5-0.727 for TGANPs gainedin an appearanceof equation (11). It is co-related with the crystalline size kindsince ~43 to 85 nm for TiO_2 and ~27 to 82 nm for TGA NPs. Similarly, Figure. 10, agrees on the diagram amid the M.I and SSA of the as-obtained TiO_2 and TGA NPs separately. The specific surface area series from 16.68 to 34.59 m^2g^{-1} for TiO_2 and 17.29-52.53 m^2g^{-1} for TGA NPsdistinctly [29]. It is detected that the M.I. is openlyrelativeto the particle size and inversely proportional to the specific surface area byminordeviances, hence the fallouts are revealed in Table. 1 and 2 compared. Linear fits in the Figure. 9 and 10 signposts the deviancies and relationsamid the three vital factors (M.I., SSA and particle/crystalline size). Thus, the detectedfallouts of the M.I. authorize the consistency and fineness of the as-obtained NPs.

3.5 Antibacterial activity

The antibacterial activity of TiO_2 and TGA NPs were examined by their ZOI for *Escherichia coli* (*E. coli*) bacterium. The antibacterial actions of ZOI wererealized for the sample (2) TiO_2 NPs and sample (3) amino-acids functioned TGA NPs exclusively as accessible in Figure 11. It was detected that the TGANPs has inhibited in the *E.*

*coli*when compared to the lesser inhibition of TiO_2 NPs.This remark might be owing to the great calcination temperature of TGA NPs and also the effective impact of amino-acids, hence that the influenced for enhanced antibacterial belongings. Operative NPs, owing to their lesser crystalline size, specifies that the superior antibacterial action [33]. In contrast, the existing work exposed that an appropriate greater antibacterial action for gram-negative (G^-) bacterium has been attained [33-34]. The highly energetic anatase TiO_2 NPs has robust oxidizing belongings that could profitably augment the microbial inhibition.

Thus, it is observed that antibacterial property, is high for TiO_2 NPs after the influence of amino-acids (TGA) NPs. Since this might be owing to the synergistic influence of glycine and alanine (amino-acids) functionalized on TiO_2 NPs with therole on a bacterial cell wall, while killed the outer cells and destruction was assisted, hence that the high antibacterial activity was assisted on TGA NPs through numerous physical and chemical routes such as (i) simulating the reaction complexes and hence enzyme inhibition by amino-acids (ii) reserve of proton translocations (iii) amino-acids functionalization in the TiO_2 NPs interrupted the cytoplasmic membrane and initiating the suspension of the proton force and subsequent in cell death [35, 36]. This advises that the growing probability of the profitable and non-toxic antibacterial bio-medical cleaning mediators.

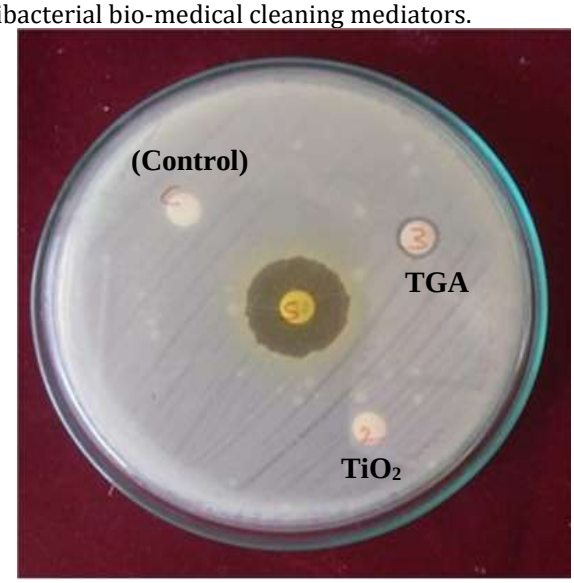

Figure. 11 The antibacterial activity of as-obtained (2) TiO_2 and (3) TGANPs against E. coli bacterium

4. Conclusion

The structural, optical and antibacterial exploration of the as-obtained TiO_2 and TGA NPs were deliberated in this existing work. The hardness and the strength of TiO_2 NPs were enhanced owing to the influence of aminoacids, which is established by power XRD readings. The typical crystalline size of TiO_2 (37.65 nm) was condensed (33.89 nm) TGA NPs owing to the impact of amino acids in the TiO_2 lattice. The specified both TiO_2 and TGA NPs were agglomerated state by uniformly assorted substances were observed and originate to be circular shape are also found in the FESEM micrographs, hence that the TGANPs have more solid than TiO_2NPs. As of the Tauc-plots, the indirect energy gap (E_g) for TiO_2NPs has shifted from ~5.5to 5.37 eV for amino-acids influenced TGA NPs. Also, the direct E_g for TiO_2NPs was shifted from 5.1 to 4.48 eV for amino-acids influenced TGA NPs, since the E_g was declined with increasing the crystalline size owing to quantum size belongings. Moreover, the consistently overlapping the E_g with narrower and agglomerated NPs were stimulated of amino-acids, which facilitate for decent bacterium - particle contact also. Besides, in the antibacterial study, the impact of amino-acids would be itemized on a major role on the surface of TiO_2 NPs hence it offers favourable results at inhibiting the *E.coli* tested bacterium. Also, it might be owing to the great calcination temperature of TGA NPs and the effective impact of active amino-acids, hence that the influenced for enhanced antibacterial belongings. Hence, the high efficiency and eco-friendly amino-acids (glycine and alanine) influenced TGANPs were validated in these upstairs results could be augmented for the various industrial applications.

Acknowledgement

The authors extend their appreciation to the Deanship of Scientific Research at King Khalid University for the financial support through the research groups program under grant number (R.G.P.2/86/41).

Conflict of Interest

The authors have declared no conflict of interest.

References

[1] H. Matsui, S. Nagano, S. Karuppusamy, M. Yoshihara J. Alloy. Compd. 468, (2009) 27-32

[2] A.B. Ali Baig, V. Rathinam, V. Ramya, Synthesis and Investigation of Fe doped SnO2 Nanoparticles for Improved Photocatalytic Activity under Visible Light and Antibacterial performances, Materials Technology. (2020) 1–13.

[3] A.M.H. Milad, L.J. Minggu, M.B. Kassim, M.Yoshihara, ceram. Int. 39, (2013) 3731-3739.

[4] K.Shanthi, P.Manikandan, C. Rani, S.Karuppusamy, Appl. Nanosci. 5,373-378 (2015).

[5] N. Suzuki, S.Karuppusamy, S. Ito. J. Appl. Electrochem. 39, 141-146 (2009)

[6] Akinola PO, Lateef A, Asafa TB, et al, Multifunctional titanium dioxide nanoparticles biofabricated via phytosynthetic route using extracts of Cola nitida: antimicrobial, dye degradation, antioxidant and anticoagulant activities, Heliyon 6:e04610 (2020).

[7] Adelere IA, Lateef A, A novel approach to the green synthesis of metallic nanoparticles: The use of agro-wastes, enzymes, and pigments, Nanotechnology Reviews, 5, (2016) 567–587

[8] Piao L, Liu Q, Li Y, Interaction of amino acids and singlewall carbon nanotubes. J Phys Chem C 116, (2012) 1724–1731

[9] M.A. Henderson: A surface science perspective on TiO2 photocatalysis.Surf. Sci. Rep. 66, (2011) 185.

[10] Perez-Torres I, Zuniga-Munoz A and Guarner-Lans V, Beneficial Effects of the Amino Acid Glycine Mini-Reviews in Medicinal Chemistry17 (2016) 15–32

[11] Umadevi, M., R. Parimaladevi, and M. Sangari. "Synthesis, characterization and photocatalytic activity of fluorine doped TiO2 nanoflakes synthesized using solid state reaction method." Spectrochimica Acta Part A: Molecular and Biomolecular Spectroscopy 120 (2014) 365-369.

[12] Hegazy A, Prouzet E, Room temperature synthesis and thermal evolution of porous nanocrystalline TiO2 anatase. Chem Mater 24 (2012) 245-254

[13] Sangari, M., M. Umadevi, J. Mayandi, K. Anitha, and Jean Patrick Pinheiro. "Photocatalytic and antimicrobial activities of fluorine doped TiO2-carbon nano cones and disc composites." Materials Science in Semiconductor Processing 31 (2015) 543-550.

[14] Unfried. K, Albercht .C, Klotz.L.O, Von Milkecz. A, Grether-Beck. S, and Schins, R.P.F. Cellular Responses to Nanoparticles: Target Structures and Mechanism Nanotechnology. 1, (2007) 52-71.

[15] Vignesh, S., Anna Lakshmi, M., Kalyana Sundar, J. Correction to: Multifunctional performance of gC3N4-BiFeO3-Cu2O hybrid nanocomposites for magnetic separable photocatalytic performance and antibacterial activity. J Mater Sci: Mater Electron 31, (2020) 13998–13999.

[16] Friedrich, Carol L., Dianne Moyles, Terry J. Beveridge, and Robert EW Hancock. "Antibacterial action of structurally diverse cationic peptides on gram-positive bacteria." Antimicrobial agents and chemotherapy 44, (2000) 2086-2092.

[17] Bani Fathima John .M.Sharfudeen, Afrin Fathima Abdul Latheef, Rose Venis Ambrose, Synthesis and Characterization of TiO2 Nanoparticles and Investigation of Antimicrobial Activities against Human Pathogens J. Pharm. Sci. & Res. Vol. 9(9), (2017), 1604-1608

[18] K. Vijayalakshmi and D. Sivaraj,Synergistic Antibacterial activity of barium doped TiO2 nanoclusters synthesized by microwave processing RSC Adv., 6, (2016), 9663–9671

[19] S. Vignesh, M. Anna Lakshmi, J. Sridhar, J. Kalyana Sundar, Construction of High Efficient g-C3N4 Nanosheets combined with Bi2MoO6-Ag Photocatalysts for Visible-Light-Driven Photocatalytic Activity and inactivation of Bacteria's, Arabian Journal of Chemistry, 13 (2020) 2439-2455.

[20] Senarathna U L N H, Fernando S S N, Gunasekara T D C P, Weerasekera M M, Hewageegana H G S P, Arachchi N D H, Siriwardena H D and Jayaweera P M, Enhanced antibacterial activity of TiO2 nanoparticle surface modified with Garcinia zeylanica extract Chemistry Central Journal11 (2017) 7

[21] S. Vignesh, J. Kalyana Sundar, Investigations of visible light driven Sn and Cu doped ZnO hybrid nanoparticles for photocatalytic performance and antibacterial activity, Applied Surface Science 449 (2018) 617-630

[22] M. Senna et al., Modification of titania nanoparticles for photocatalytic antibacterial activity via a colloidal route with glycine and subsequent annealing J. Mater. Res., 28, (2013)

[23] Jawahar, A., T. Mathavan, M. Kumara Dhas, and A. Milton Franklin Benial. "Preparation and characterization of oxidized multi-walled carbon nanotubes and glycine functionalized multi-walled carbon nanotubes." Fullerenes, Nanotubes and Carbon Nanostructures 23, (2015) 583-590.

[24] Hanaor DAH, Sorrel CC, Review of the Anatse to rutile phase transformation. J Mater Sci 46 (2011) 855-874.

[25] Abbas, Nadir, Godlisten N. Shao, M. Salman Haider, Syed Muhammad Imran, Sung Soo Park, Sun-Jeong Jeon, and HeeTaik Kim. "Inexpensive sol-gel synthesis of multiwalled carbon nanotube-TiO2 hybrids for high performance antibacterial materials." Materials Science and Engineering: C 68 (2016): 780-788.

[26] Umadevi, M., M. Sangari, R. Parimaladevi, A. Sivanantham, and J. Mayandi. "Enhanced photocatalytic, antimicrobial activity and photovoltaic characteristics of fluorine doped TiO2 synthesized under ultrasound irradiation." Journal of Fluorine Chemistry 156 (2013): 209-213.

[27] Jaiakumar, Thilagavathy, et al. "Synergistic effect of MgO/Ag co-doping on TiO2 for efficient antibacterial agents." Materials Letters 184 (2016): 82-87.

[28] Senna, Mamoru, et al. "Modification of titania nanoparticles for photocatalytic antibacterial activity via a colloidal route with glycine and subsequent annealing." Journal of Materials Research 28.3 (2013): 354-361.

[29] Ibrahim. A, Abdul-Hassan, Ahmed K.Abbas, IsamM.Ibrahim and Zinah S.Shallal, Characterization and Antimicrobial Effects of Titanium dioxide Nanoparticles Produced by Laser Ablation, 8 (2018) 14286-14292.

[30] A.B. Ali Baig, V. Rathinam, J. Palaninathan, Fabrication of Zr-doped SnO2 nanoparticles with synergistic influence for improved visible-light

photocatalytic action and antibacterial performance, Applied Water Science. 10 (2020) 54.

[31] Kumar, Sandeep, et al. "Synthesis, characterization and antimicrobial activity of nano titanium (IV) mixed ligand complex." Materials Focus 2(6) (2013): 475-481.

[32] S. Suganthi, S. Vignesh, S. Mohanapriya J.K. Sundar, V. Raj, Microwave-assisted synthesis of l-histidine capped silver nanoparticles for enhanced photocatalytic activity under visible light and effectual antibacterial performance, J Mater Sci: Mater Electron, 30(16), (2019) 15168-15183

[33] Abbas N, Shao GN, Haider MS, Imran SM, Park SS, Jeon SJ, Kima HT, Inexpensive sol–gel synthesis of multiwalled carbon nanotube-TiO2 hybrids for high performance antibacterial materials. Mater Sci Eng C 68 (2016) 780–788

[34] Mahalingam, Umadevi, et al. "Fluorinated TiO2-doped, glycine-functionalized MWCNTs for high-performance antibacterial agents." Carbon Letters 29.1 (2019): 65-68.

[35] K. Gnanamoorthi, M. Balakrishnan, E.R. Kumar, R. Mariappan, T. Prakash, A.A. Baig, M. Prakasam, Structural and Morphological of Ti Doped ZrO2 Nanoparticles Synthesized by a Microwave Irradiation Method , Journal of Advanced Physics. 7 (2018) 199–204.

[36] S. Kavitha, N. Jayamani, D. Barathi, A study on preparation of unique TiO2/Cu2O nanocomposite with highly efficient photocatalytic reactivity under visible-light irradiation, Materials Technology. (2020) 1–14.